Enhancement of growth of MOF MIL-68(Al) thin films on porous alumina tubes using different linking agents

Adelaida Perea-Cachero,[a] Pablo Calvo,[a] Enrique Romero,[b] Carlos Téllez[a] and Joaquín Coronas*[a]

Chemical and Environmental Engineering Department, Universidad de Zaragoza, 50018 Zaragoza, Spain

[a] Instituto de Nanociencia de Aragón (INA), Universidad de Zaragoza, 50018 Zaragoza, Spain

[b] Aragón Institute of Engineering Research (I3A), Universidad de Zaragoza, 50018 Zaragoza, Spain

*Corresponding author: coronas@unizar.es.

Abstract

The preparation of MIL-68(Al) films on the inner surface of alumina tubes is reported. As the direct deposition of the MOF on bare alumina gave poor adhesion results, three different linking agents were employed in order to achieve a good MOF-support interaction. Colloidal silica LUDOX®, zeolite silicalite-1 and natural polysaccharide chitosan were chosen as binders because they contain potential functional groups (hydroxyl, amino, ether) which can establish hydrogen bonds. While colloidal silica led to non-continuous MOF layers, silicalite-1 and chitosan gave rise to uniform and well-anchored films, as confirmed by the different characterization techniques used to study the MOF layer. Single gas permeation experiments were carried out to determine the quality and ideal efficiency of the membranes prepared with silicalite-1 and chitosan. The results for the MIL-68(Al)/silicalite-1 membranes evidenced the existence of macrodefects. However, no cracks were found when chitosan was used as a linking agent and the gas flow through the MIL-68(Al)/chitosan membranes clearly followed Knudsen diffusion.

Introduction

Membrane-based separations have gained attention in recent years due to their advantages compared to conventional methods, such as cost and energy savings, ease of processing, reliability and smaller carbon footprint.[1-3] Commercial gas separations through membrane technology are controlled by polymeric membranes owing to their low cost, high processability and mechanical stability.[1, 3, 4] Nonetheless, there is a trade-off between selectivity and permeability, short lifetimes and low thermal and chemical stabilities.[1, 5] These shortcomings usually restrict the use of polymeric membranes in the separation of mixtures of non-condensable gases (CO_2/N_2, CO_2/CH_4, H_2/N_2, H_2/CO_2, etc.),[1, 6] hence the need for alternatives. Continuous thin films or membranes are formed by the deposition of porous particles on substrates of distinct materials (silica, alumina, titania, graphite, stainless steel, brass, Au, etc.) and shapes (plates, tubes, hollow fibers, etc.) to create uniform and well-intergrown layers.[1, 5, 7, 8] In the case of metal-organic framework (MOF) films, their homogeneity, uniformity, thickness and crystal shape could influence their chemical and physical features.[9] In addition, the high porosity and regular pore structure of MOFs may result in high selectivities and fluxes.[10] These properties, besides their relative large chemical and thermal stability, have stimulated research into their use not only for gas separations, but also for membrane reactors and advanced applications in optics and electronics.[11] Besides MOFs, selective materials for continuous membranes mainly comprise zeolites. Despite their chemical and thermal stability in harsh environments, zeolites show a limited range of pore sizes, are expensive (in part due to the high probability of the presence of defects) and have the disadvantages of complex fabrication and poor chemical functionalization.[1, 2, 12] On the other hand, MOFs present an extensive range of available pore sizes and shapes and have a high degree of chemical tunability of the pore surfaces which enables tailoring of their chemical and adsorption properties.[13] MOFs, or porous coordination polymers (PCPs), are formed by the coordination of metal ions or clusters and organic linkers originating porous structures.[14] There has been increasing interest in research into MOFs in recent years because of their remarkable features such as high surface areas and pore volumes, chemical and thermal stabilities and structural flexibility,[1] all of which facilitate their use, for instance, in gas separation[15] and storage,[16, 17] adsorption,[18] drug delivery[17] and catalysis.[17, 19]

The fabrication of MOF thin films or membranes is not a trivial matter. The major problems with MOF membranes are the poor MOF-support interaction and moisture stability, as well as the presence of macroscopic defects.[6] According to several authors, the MOF-substrate binding could be enhanced through the functionalization of the support surfaces,[20] the use of polymer linkers[21] and carbon/graphite coatings[22], and the pre-attachment of crystal seeds.[23] The moisture instability may be reduced *via* post-functionalization methods incorporating hydrophobic groups into the MOF skeletons.[24] Macroscopic cracks could be avoided by a slow cooling of the membranes after synthesis,[23] careful activation by gradual solvent-exchanges and/or slow solvent evaporations,[25] and using polymer supports with better chemical matching with MOFs.[8]

Here, the synthesis of MIL-68(Al) membranes on alumina tubes is reported. MIL-68 (MIL for *Matériaux de l'Institute Lavoisier*) is a MOF constructed by infinite chains of octahedral $MO_4(OH)_2$ building units (M: V, Al, Sc, In, Ga, Fe) connected through hydroxyl groups placed at

trans apical positions (figure 1a).[9, 26, 27] Inorganic chains are linked by terephthalate ligands delimiting two kinds of one-dimensional pores: triangular and hexagonal channels of 0.6 nm and 1.6-1.7 nm in opening diameter, respectively (figure 1b).[28] The high thermal and chemical stability of MIL-68(Al) motivated its use as a selective material. Besides, its two different pore sizes could benefit the separation of gas mixtures.[9, 26] Only a few examples incorporating MIL-68(Al) as a selective material for separation applications are found in the literature. Echaide-Górriz *et al*. included MIL-68(Al) nanoparticles into thin film nanocomposite membranes for organic solvent nanofiltration.[29] Regarding the separation of gas mixtures, Seoane *et al*. prepared mixed matrix membranes (MMMs) embedding nanosized MIL-68(Al) crystals in polysulfone for H_2/CH_4 and CO_2/CH_4 separation, improving the selectivity from the pure polysulfone membrane.[27] Dong *et al*. also fabricated MMMs with MIL-68(Al) as the filler but they selected Matrimid® as the polymeric matrix, obtaining a CO_2/CH_4 selectivity of 79.0.[30] Considering thin films based on the MOF MIL-68, Liu *et al*. studied the influence of different parameters (reaction temperature and time and concentration of the reaction solution) to control the MIL-68(In) film thickness and morphology.[9] However, they did not explore any application for the synthesized membranes. In the present work, poor crystal adhesion was achieved when preparing the MOF layer directly on the bare supports. Therefore, colloidal silica LUDOX®, zeolite silicalite-1 and polymeric carbohydrate chitosan were chosen as intermediate agents in order to obtain continuous MIL-68(Al) membranes. Uniform and well-anchored MOF films were only achieved in the cases using silicalite-1 and chitosan. To study the quality of the membranes, single gas permeation tests were carried out. Permeation determined the existence of defects in MOF/zeolite membranes and Knudsen diffusion for the gas transport through chitosan-based membranes.

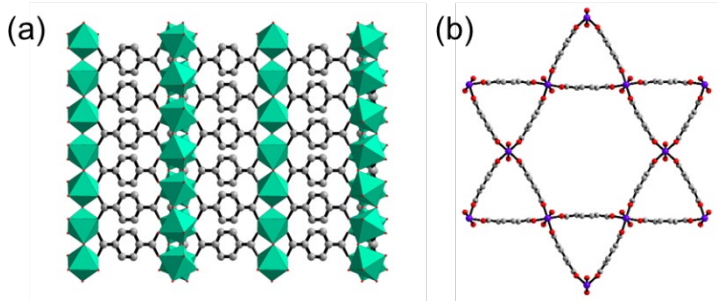

Figure 1. Structure of MIL-68.[31] (a) Representation of the inorganic $MO_4(OH)_2$ octahedra chains along the (1 1 0) direction. (b) View of the triangular and hexagonal unidimensional pores along the (0 0 1) direction. M, C and O atoms are depicted in blue, grey and red, respectively. H atoms are omitted.

Results and discussion

MIL-68(Al) on bare alumina supports

Direct syntheses of MIL-68(Al) on the bare alumina support resulted in non-covered surfaces. The same conditions as described in the Experimental section were tried for 18.5 and 72 h (figure S1a and b). With a reaction time of 18.5 h, few crystals were formed between large alumina grains. After 72 h, MOF crystals also grew on top of alumina grains, but their size was very small whereas the crystals between grains were bigger than those at 18.5 h. These results show that

the MIL-68(Al) growth benefitted from the defects at the alumina grain boundaries. Moreover, the MOF layer of the sample at 72 h was cracked all over the support surface. The cracks are thought to have been caused during the solvent evaporation.

MIL-68(Al) on LUDOX®-treated supports

As a homogeneous MIL-68(Al) layer was difficult to achieve on the naked alumina tubes, it was thought that an intermediate agent could interact with the alumina surface as well as the MOF to accomplish an effective bond between both components of the membrane. The same synthesis carried out on the bare substrates was accomplished on supports pre-treated with colloidal silica (LUDOX®). The LUDOX® suspension contains nanometric silica particles dispersed in water. It was hypothesized that silica particles would be readily fixed to alumina as a thin coating of amorphous silica and could bind to MOF crystals through hydroxyl groups. ESEM images for reaction times of 18.5 h and 72 h are displayed in figures S1c and S1d. They are very similar to images from the direct syntheses on naked supports. For 18.5 h, MIL-68(Al) was placed on voids between alumina grains and only a few crystals appeared on top of grains without achieving a uniform layer. In contrast, for 72 h, small crystals formed a layer on the whole support surface, although evident cracks are observed. The cracks might have been provoked by DMF evaporation after the MIL-68(Al) layer formation. No defects relating to poor adhesion were found by ESEM. MOF preferentially grew in spaces between alumina grains as in the previous case of MIL-68(Al) on naked supports. The corresponding PXRD pattern (figure 2) reveals two weak reflections (2θ = 8.9 and 10.2°) associated to the peaks placed at the 2θ values of 9.1 and 10.0° of the MIL-68(Al)_as. The high alumina influence is also visible in the pattern (orange lines and asterisks).

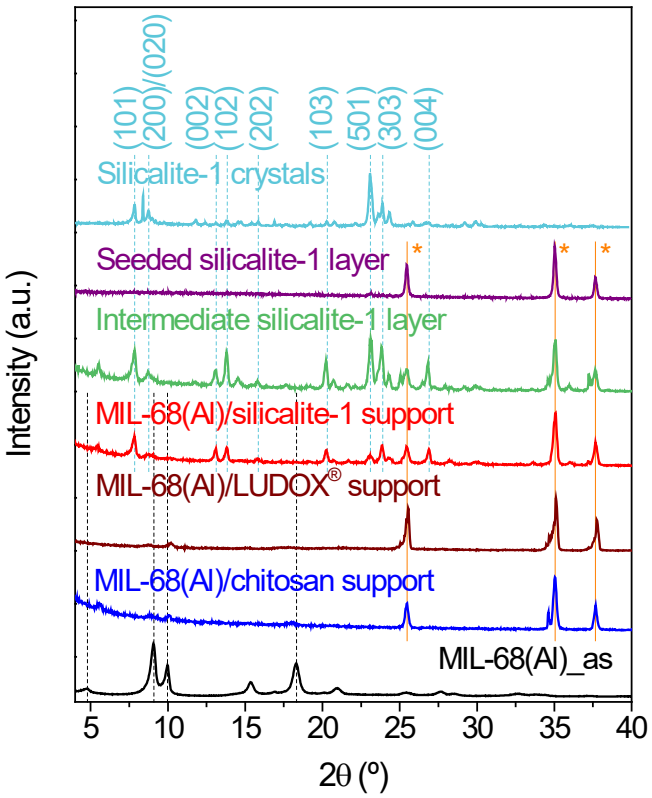

Figure 2. PXRD patterns of as-made silicalite-1 and MIL-68(Al), the seeded and intermediate silicalite-1 layers as well as the as-synthesized MOF layer prepared on alumina (2 cm-long tubes) coated with LUDOX®, silicalite-1 and chitosan. Signals corresponding to alumina are marked by orange lines and asterisks.

Hybrid MIL-68(Al)/silicalite-1 membranes

As seen above, accomplishing a uniform and well-adhered MIL-68(Al) layer on alumina tubes is a key issue. Even using an intermediate agent like LUDOX®, with a high concentration of hydroxyl groups, was not enough for this purpose. This encouraged us to study other options for intermediate linking agents, including silicalite-1. Silicalite-1 is a hydrophobic zeolite with the MFI type topology composed of pure silica.[32] It was chosen mainly for three reasons. (1) Hydroxyl groups were supposed to serve as a means to anchor MOF crystals (the hydroxyl group concentration in the silicalite-1 is lower than in the amorphous silica derived from LUDOX®). (2) The less rough surface of a silicalite-1 layer in comparison with that of an alumina tube could be crucial for a better MOF coverage. (3) A uniform and well-intergrown silicalite-1 intermediate layer could enhance the gas separation efficiency of the final MOF/zeolite membranes, as in the work of Yeo *et al*.[33] where a hybrid membrane was fabricated by deposition of zeolite T on an intermediate ZIF-8 layer. The zeolite T/ZIF-8 membrane improved the CO_2/CH_4 selectivity of the ZIF-8 and zeolite T membranes (193.0 *vs*. 3.0 and 49.0, respectively) because of the double multiplying effect of CH_4 sieving.

As mentioned in the Experimental section, the silicalite-1 layer was prepared by means of a secondary growth method. Seeding was carried out following a dip-coating procedure. Figures 3a and 3b show SEM and ESEM images of the silicalite-1 seeds obtained from the seed suspension and the inner surface of a seeded support, respectively. The seeds had an irregular morphology with a size ranging from 170 to 225 nm and covered the surface uniformly. After secondary growth, a continuous silicalite-1 polycrystalline layer was formed onto the substrate surface (figure 3c). As expected, the silicalite-1 crystals had a morphology of elongated hexagonal prisms (see figure S2). They were apparently oriented with the *c* axis perpendicular to the support. The ESEM images also exhibit some crystals stuck on the top of the zeolite layer.

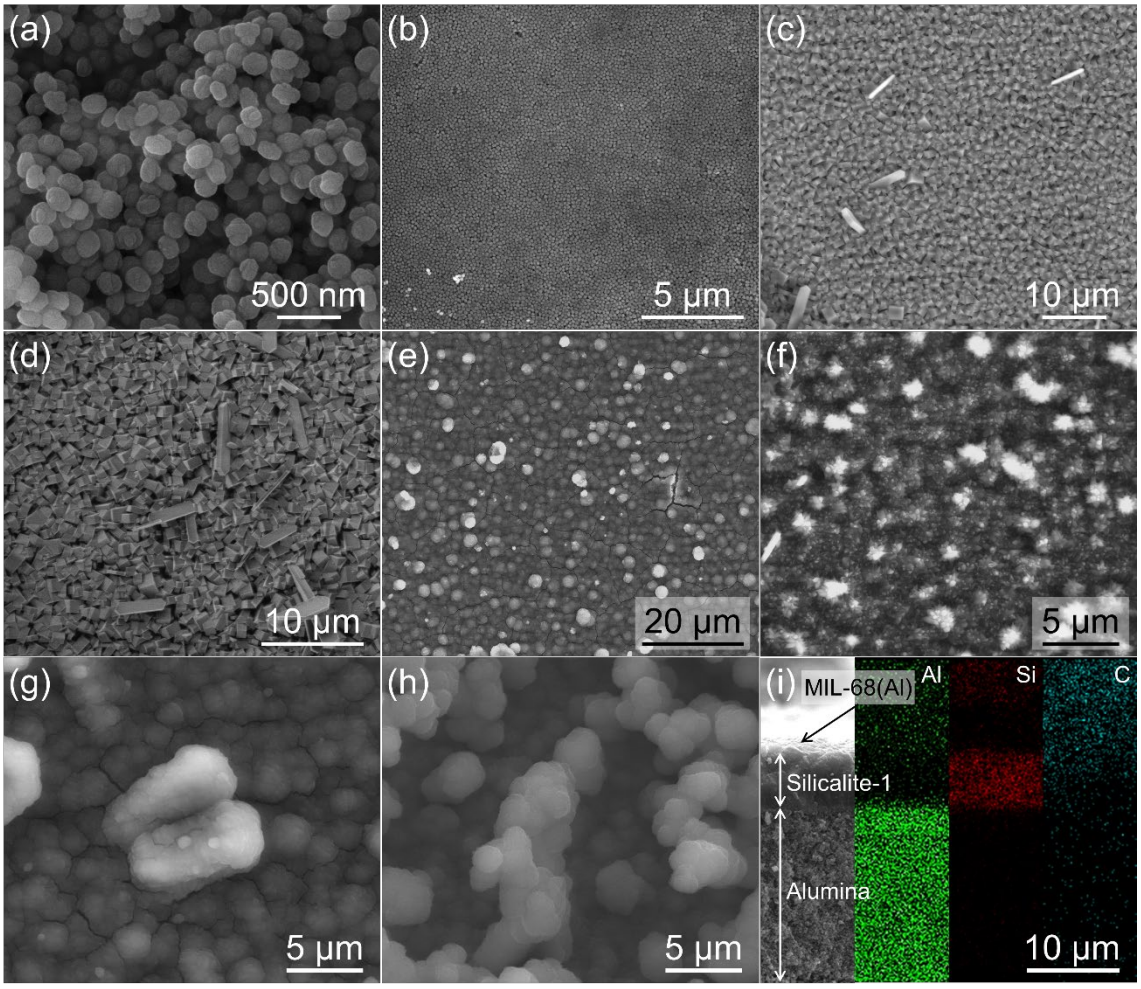

Figure 3. (a) SEM image of the silicalite-1 seeds from a seeding suspension. ESEM images of (b) a silicalite-1 seed layer, (c) an uncalcined and (d) a calcined (380 °C) intermediate silicalite-1 layer. (e) ESEM image of as-made MIL-68(Al) on a non-calcined silicalite-1 layer (cracks were produced by the electron beam). ESEM images of activated MOF/zeolite-coated supports with the silicalite-1 layer calcined at (f) 380 and (g) 450 °C. (h) ESEM image of an activated MOF/silicalite-1-coated support with the zeolite calcined at 380 °C prepared for reproducibility purposes. (i) Cross sectional ESEM image and elemental EDX mappings (Al, green; Si, red; C, cyan) of the hybrid MOF/silicalite-1 composite with the zeolite layer calcined at 380 °C. Images from (b) to (i) were taken from samples prepared on 2 cm-long supports.

As the silicalite-1 seeded layer was very thin compared to the alumina substrate, only a weak peak corresponding to the (5 0 1) reflection arose in the PXRD pattern (figure 2). For the intermediate silicalite-1 layer, peaks with (1 0 *l*), (0 0 2) and (*h* 0 *h*) orientations predominated indicating two main crystal arrangements (figure 2), as in the work reported by Lai *et al*.[34] In the first, the *b* axis is parallel to the support surface. In the second, the *c* axis is perpendicular to the substrate. These results are in accordance with the ESEM images shown above.

The MIL-68(Al) growth on the non-calcined silicalite-1 layer led to a complete and uniform coverage (figure 3e). MIL-68(Al) crystals are observed generally to have the shape of short needles as part of spherical aggregates. It is worth mentioning that cracks were produced by the electron beam of the microscope. Before MIL-68(Al) film formation, the calcination of the silicalite-1 layer was required to remove the template (TPA^+) from the zeolitic pores, otherwise they would not allow the gas transport through the final composite membrane. Two calcination temperatures were tested: 380 and 450 °C. ESEM images of the MOF films obtained are depicted in figures 3f and 3g. Although crystals completely covered the support surface in both cases, the calcination temperature of 450 °C resulted in the formation of cracks and MOF aggregates adhered to the MIL-68(Al) film. When the silicalite-1 layer was calcined at 380 °C, cracks were not visible. In this sample, MOF crystals appeared with a petal morphology and their length varied between 500 and 800 nm. Silicalite-1 is usually calcined at high temperatures (450-600 °C) to ensure the complete elimination of the template used in its synthesis.[35] Silanol groups (Si-O-H) are placed on the external surface of zeolite crystals and at framework defects.[36] Besides generating porosity, the calcination of zeolites causes their dehydroxylation, i.e. water molecules are removed upon heating with the destruction of superficial silanol bonds and the formation of siloxane groups (Si-O-Si).[37] As a consequence, the total number of hydroxyl groups decreases, although the number of terminal silanol groups increases.[38] Hydroxyl groups were thought to fix MIL-68(Al) particles. Therefore, the calcination temperature should be chosen so as to provide a trade-off between the presence of hydroxyl groups and the degree of zeolite activation for proper permeation properties. This explains the unsuccessful result achieved when adhering MOF crystals with a calcination temperature of 450 °C, the apparently high quality of the MIL-68(Al) film at 380 °C and the high coverage on the non-calcined silicalite-1 layer (including a larger number of hydroxyl groups than the zeolite layers calcined at 380 and 450 °C).

In order to check whether a temperature of 380 °C was high enough to release TPA^+ molecules, the BET surface area of calcined silicalite-1 powder was determined. The BET area was 374 m^2 g^{-1}, approaching the value for a sample calcined at 450 °C (384 m^2 g^{-1}) (figure S3) and the typical value for MFI molecular sieves (approximately, 400 m^2 g^{-1}).[39] This confirms the high degree of activation. ESEM images of the zeolite layer treated at 380 °C showed that calcination did not provoke cracks (figure 3d). The ESEM and EDX cross section views of the hybrid support after silicalite-1 calcination at 380 °C are shown in figure 3i. The alumina support and the intermediate silicalite-1 layer were clearly differentiated while the MIL-68(Al) film was barely perceived. EDX analysis allows a top zone to be identified with higher Al and C contents than those of the silicalite-1 layer corresponding to the MOF. The zeolite and MOF layers had thicknesses of around 6.4 and 0.8 µm, respectively. Furthermore, silicalite-1 and MIL-68(Al) crystals were observed to be well-intergrown and well-anchored to alumina and zeolite, respectively. Thus, the lower roughness of the silicalite-1 layer in comparison with that of the alumina surface and

the presence of some external hydroxyl groups facilitated and prompted the bonding to MIL-68(Al) crystals.

As the MOF layer was too thin, the PXRD pattern of the MIL-68(Al) film growth on the silicalite-1-modified support (figure 2) did not reveal any peak assignable to the MOF. Only silicalite-1 and alumina contributions were seen, although the reflection at 2θ = 5.4° could have been due to MIL-68(Al) (2θ = 4.8°). FTIR and ATR-FTIR studies were useful to confirm the MOF layer formation. Figure S4 displays the spectra of the MIL-68(Al)/silicalite-1 composite and MIL-68(Al)_as. Both were in good agreement and exhibited the most characteristic signals of MIL-68(Al). The appearance of the band at 1674 cm^{-1} in MIL-68(Al)_as corresponded to the carbonyl group from DMF, confirming the existence of solvent molecules in the MOF pores. The band relating to the carbonyl group of free terephthalic acid (placed at *ca*. 1700 cm^{-1})[28] could have been overlapped by the carbonyl signal from DMF. In the spectrum of the non-activated MIL-68(Al) film deposited on the zeolite-coated support, a small band from DMF arose at 1669 cm^{-1} and the weak signal at 1701 cm^{-1} was assigned to free terephthalic acid. This means that the activation of the MIL-68(Al) film was needed in order to release the guest molecules from the pores.

Reproducibility is a difficult task when obtaining continuous thin films, owing to the number of variables involved during their fabrication.[12] A second hybrid MOF/zeolite-coated support (denoted by *_r*) was synthesized and activated following the method reported here to study the reproducibility. The MIL-68(Al) crystals were around 475-600 nm long and did not possess the petal shape seen in the first sample (see figure 3h). Although the crystals were shorter than those of the first MIL-68(Al)/silicalite-1-coated support (500-800 nm), the spherical aggregates were visibly larger and more numerous. These differences demonstrate, as mentioned above, that achieving two identical MOF membranes is complicated. In spite of this, a continuous MOF film was formed. Regarding activation, the ATR-FTIR spectrum shows that DMF was released from the MOF skeleton whereas a small amount of free terephthalic acid still remained (figure S4). As confirmed by ESEM, the activation process did not produce any cracks or defects on the MOF film surface (figure 3h).

Taking into account the success in preparing the MOF/zeolite layer on 2 cm-supports, the synthesis and activation processes detailed in this paper were scaled up to 8 cm-tubes for single gas permeation experiments. A sample of powder MIL-68(Al) obtained in the synthesis of one scaled membrane was similarly activated (MIL-68(Al)_sil). DMF as well as free terephthalic acid molecules remained occluded in the pores, as seen by FTIR (carbonyl bands at 1672 and 1703 cm^{-1}) and TGA (mass losses of 9.1 and 2.2 % at 60-300 °C and 300-370 °C, respectively), indicating that the membrane could not be totally activated (figure S4 and S5). Nevertheless, a comparative graph of N_2 permeances at different transmembrane pressures for bare tubes, silicalite-1 membranes (before MOF deposition) and MOF/zeolite membranes is depicted in figure S6. In the MOF/zeolite membrane, two different materials having distinct topologies (Kagomé for MIL-68(Al)[40] and MFI for silicalite-1)[41] are combined. There are several other examples of two distinct materials being used as separated layers or core-shells to form membranes (zeolite/zeolite,[42] ZIF/ZIF,[8] MOF/MOF,[43] zeolite/ZIF,[44] silica/ZIF,[45] etc.). Since a single silicalite-1 synthesis on the seeded alumina gave poor permeation results (not shown), two more syntheses were carried out before calcination and MOF deposition to fabricate the

membranes. As can be seen in figure S6, the calcined silicalite-1 membrane gave a permeance two orders of magnitude less than that of the bare tube due to the zeolite formation on the alumina surface (10^{-7} *vs*. 10^{-5} mol m^{-2} s^{-1} Pa^{-1}). The Knudsen contribution was 74.5 % (table S1). This value is low in comparison with reported values for other silicalite-1 membranes.[46] We have to say that the goal here was not to obtain a high quality silicalite-1 membrane but rather an appropriate modified alumina surface for the growth of the MOF. It is thought that calcination at 380 °C was not enough for full TPA^+ removal, so that some template molecules remained occluded in the zeolite pores after calcination. The N_2 permeance of the activated MOF/zeolite membrane (10^{-6} mol m^{-2} s^{-1} Pa^{-1}) was higher than that of the zeolite membrane and the Knudsen contribution decreased (74.5 *vs*. 51.6 %, table S1). The increasing trend in the permeance of N_2 and the low Knudsen percentage pointed to the existence of macroscopic defects produced during the synthesis of the MOF. In spite of the good results in terms of adhesion and homogeneity observed by SEM, EDX and ATR-FTIR, the permeation experiments were unsuccessful. Although these membranes are not adequate for gas separation, they could be used, for instance, in sensors[47] or in pervaporation, where the presence of hydrophilic defects is not so significant when, for example, dehydrating solvents.[48]

MIL-68(Al) films on chitosan-coated supports

Chitosan is an abundant biodegradable copolymer.[49, 50] It comprises N-acetyl-D-glucosamine and D-glucosamine units in different ratios depending on the degree of acetylation (figure S7).[49] It was thought that chitosan could bind through its hydroxyl, amino and/or ether groups to MIL-68(Al) and alumina by means of hydrogen bonds.[51] This biopolymer has previously been used to bind different kinds of materials in order to create thin films and membranes. For instance, Zhou *et al.* employed chitosan as a polymer binder to assemble *b*-oriented silicalite-1 monolayers on glass plates[51] and Zhou *et al*. synthesized HKUST-1 membranes by a secondary growth method fixing the seeds on chitosan-coated alumina hollow fibers.[52]

ESEM images of the 2 cm-long supports coated by MIL-68(Al) using chitosan as a linking agent are shown in figure 4. MIL-68(Al) crystals covered the whole surface and formed spherical agglomerates (figure 4a), as in the case of the MOF/zeolite-coated supports. The crystals were needle-shaped and around 400-700 nm in size, slightly shorter than those of the MOF/zeolite composite (500-800 nm). The cross sectional ESEM image shows a thin MOF layer (the bright top layer) readily distinguished by EDX mappings (figure 4d). The MOF layer on chitosan-alumina was thicker than that synthesized on zeolite-alumina (1.2 *vs*. 0.8 µm). Chitosan formed a thin layer on the support surface and penetrated into the more external pores of the alumina. Otherwise, the corresponding coating would be observed by SEM and EDX of the cross section. Tiny chitosan particles completely coated the alumina, smoothing the surface (figure S1e and S1f). The PXRD pattern of a MIL-68(Al) film on a chitosan-treated support displays three weak signals (2θ = 8.9, 10.1 and 18.1°) that can be attributed to the reflections at the 2θ angles of 9.1, 10.0 and 18.3° from MIL-68(Al)_as, although they appeared slightly displaced towards lower 2θ values (see figure 2). The first peak (at 2θ = 5.4°) might also come from MIL-68(Al). The alumina contribution is clearly noticeable (represented by orange lines and asterisks). The ATR-FTIR spectrum of the activated MIL-68(Al) film on a chitosan-coated support matches that of MIL-68(Al)_as, confirming the formation of the desired MOF (figure S4). The spectrum presents two weak bands related to the carbonyl groups from free terephthalic acid and DMF, i.e. a full

activation was not achieved. The activation process did not provoke any damage to the MOF film but led to smoothed crystal edges, as confirmed by ESEM (figure 4b). The light zone and the small cracks in the middle of the image were caused by the electron beam. Another MIL-68(Al)/chitosan-coated support was prepared to study the reproducibility of the process. The MOF crystals formed on the chitosan polymer were well-defined and shorter (165-300 nm) than those of the initial sample (figure 4c). The film was also continuous and fractures were not observed. These facts highlight the difficulty found when fabricating MOF thin films, as in the case of using silicalite-1 as a binder.

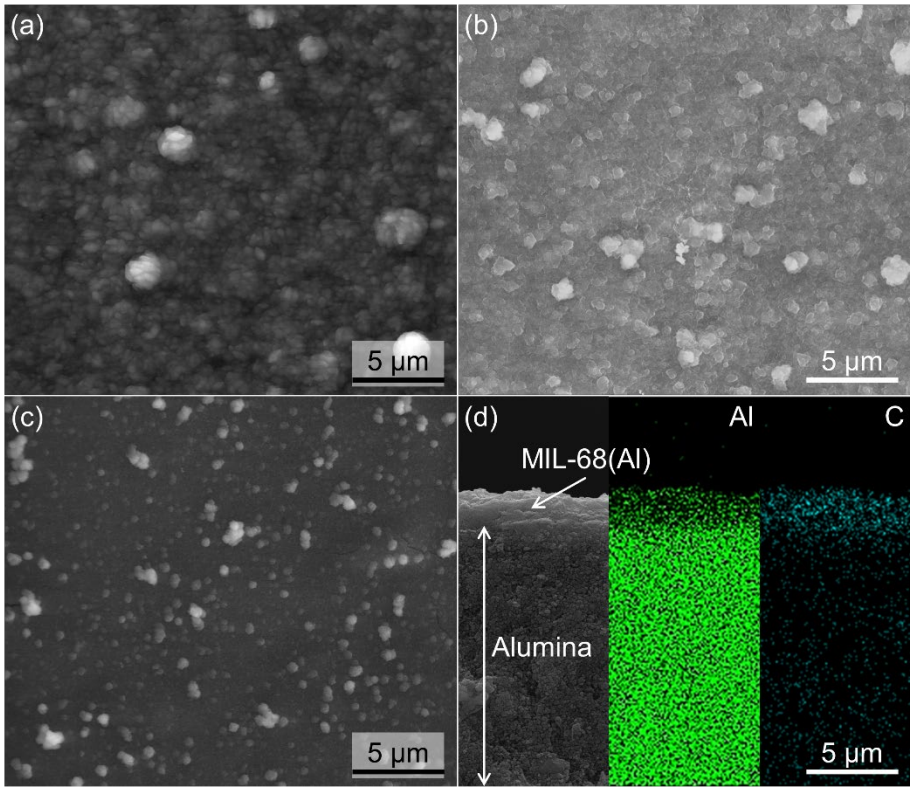

Figure 4. Top-view ESEM images of (a) a MIL-68(Al) film on a chitosan-coated alumina support, (b) the same sample but activated, and (c) a reproduced MIL-68(Al)/chitosan-coated support. (d) Cross section ESEM image of the as-made MIL-68(Al)/chitosan-coated support with EDX mappings (Al, green; C, cyan). The ESEM images and EDX mappings were obtained from samples supported on 2 cm-long tubes.

Bearing in mind the characterization results, the chitosan procedure was scaled up to 8 cm-tubes so as to carry out permeation experiments. The degree of activation was assessed by FTIR spectroscopy (figure S4). The MIL-68(Al) powder product obtained when preparing one MOF/chitosan membrane was activated employing the same method, giving MIL-68(Al)_chi. MIL-68(Al)_chi powder presented a very weak band corresponding to free terephthalic acid and no signal from DMF was found. However, the corresponding TGA curve showed weight losses of 3.0 and 3.5 % at 145-260 °C and 260-360 °C assigned to DMF and terephthalic acid release, respectively, indicating small amounts of both guest molecules. The quality of the membranes was studied by N_2 permeation at 35 °C at several transmembrane pressure drops (figure S6). As observed, the N_2 flux was mostly independent of the pressure, so that the viscous flow had a small influence on the gas transport mechanism and could be negligible. The N_2 permeance was

similar to that of the MOF/zeolite membranes (10^{-6} mol m^{-2} s^{-1} Pa^{-1}). The Knudsen contribution was quite different; 96.8 *vs*. 51.6 % for membranes prepared with chitosan and silicalite-1 as intermediate agents, respectively (table S1). This underlines the quality of the MIL-68(Al) films synthesized on chitosan-coated alumina. Single gas permeances of H_2, CO_2 and CH_4 at different transmembrane pressures were also determined and the ideal selectivities for the H_2/CH_4, H_2/CO_2, CO_2/N_2 and CO_2/CH_4 pairs were calculated. The permeance values of these gas molecules followed the same trend as N_2, supporting the good quality of the membranes which did not contain macroscopic defects (figure S8). As seen in figure 5, the ideal selectivities were near the corresponding Knudsen values for all the gas mixtures. The greater difference was found for H_2/CO_2 due to the preferential adsorption of CO_2 by the MOF.[53] The relationship when plotting permeances (at 35 °C and 1 bar) against the inverse square roots of the molecular weight of all the gases was linear, as expected for Knudsen diffusion (figure 6). The preferential adsorption of CO_2 is also seen in this graph; the permeance of CO_2 differed slightly from a pure Knudsen flow (dashed line).[53] The evidence shows that the flow of gases through the activated MIL-68(Al)/chitosan membranes was mainly governed by the Knudsen mechanism. This is due to the larger size of MIL-68(Al) pores (0.6 and 1.6-1.7 nm) in comparison with the kinetic diameters of the gas molecules (0.29, 0.33, 0.36 and 0.38 nm for H_2, CO_2, N_2 and CH_4, respectively).[11]

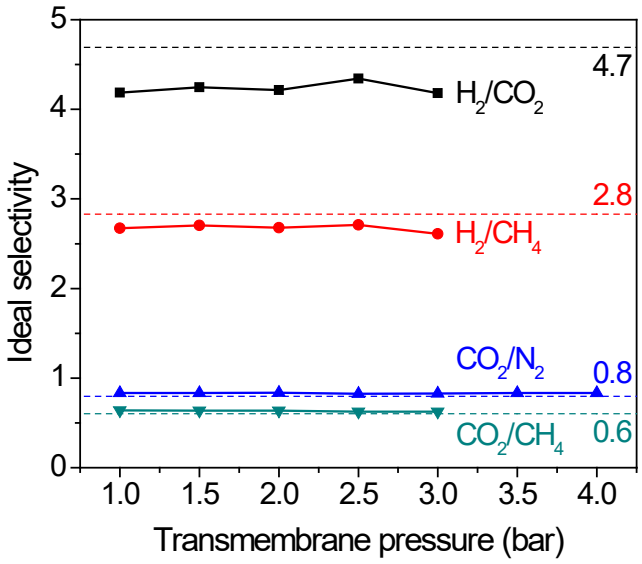

Figure 5. Ideal selectivities of different gas pairs *vs*. the transmembrane pressure difference at 35 °C in comparison with the Knudsen selectivity (dashed lines) for an activated MIL-68(Al)/chitosan membrane.

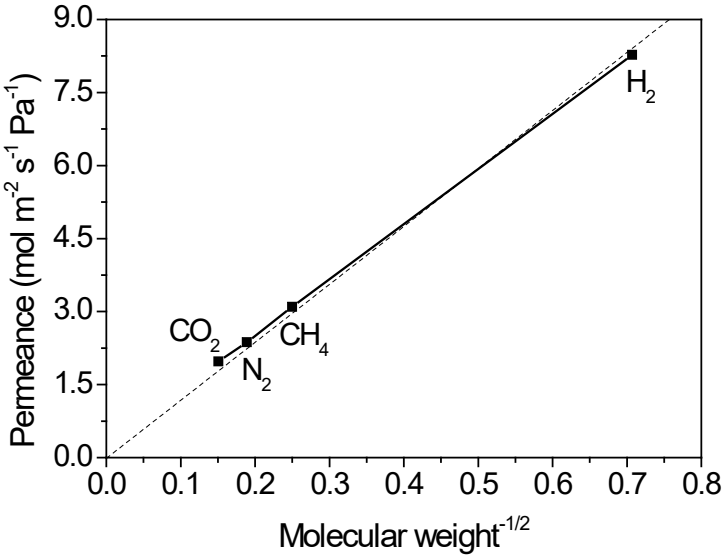

Figure 6. Permeances of H_2, CH_4, N_2 and CO_2 against the inverse of the square root of the corresponding molecular weight at 35 °C and 1 bar of pressure difference for an activated MIL-68(Al)/chitosan membrane.

Conclusions

This work deals with the preparation of MIL-68(Al) films on the inner surface of alumina tubes. Since MIL-68(Al) was poorly adhered to the bare alumina, different binding agents (colloidal silica LUDOX®, silicalite-1 and chitosan) were used to improve the MOF-support interaction. The hydroxyl, amino and ether groups of these binders were thought to create hydrogen bonds between alumina and MIL-68(Al), achieving a good linkage. Thorough characterization was carried out to study the uniform coverage of the MOF layers obtained. Only silicalite-1 and chitosan agents gave homogeneous and well-anchored MOF films. It is worth mentioning that MIL-68(Al)/silicalite-1 membranes combine two crystalline materials with different topologies. Nonetheless, single gas permeation experiments were unsuccessful as the high influence of the viscous flow indicated the presence of macroscopic defects. In addition, single gas permeances of H_2, CH_4, N_2 and CO_2 demonstrated that no cracks or defects were present in the MIL-68(Al)/chitosan membranes. The chitosan structure comprises a large number of functional groups prone to establish hydrogen bonds, improving the anchorage between the alumina surface and the MOF and, thus, the MIL-68(Al) film quality. The Knudsen diffusion mechanism governed the gas transport through this type of membrane with a minor contribution of preferential adsorption of CO_2. The difficulties of MOF thin film and membrane preparation is evident considering the results described here. Nevertheless, the use of distinct kinds of materials rich in functional groups capable of forming hydrogen bonds, such as zeolites and biopolymers, facilitates the anchorage of MOFs on porous supports, achieving continuous films suitable for application in a number of fields including gas separation (studied here), catalysis, pervaporation, sensoring, optics, electronics and magnetism.

Experimental section

<u>General methods and materials</u>

Aluminum chloride hexahydrate ($AlCl_3 \cdot 6H_2O$, 99 %, Sigma-Aldrich), terephthalic acid (C_6H_4-1,4-$(CO_2H)_2$, 98 %, Aldrich), methanol (CH_3OH, 99.9 %, Scharlau), *N*,*N*-dimethylformamide ($HCON(CH_3)_2$, 99.95 %, Scharlau), potassium hydroxide (KOH, 85 %, Alfa Aesar), tetraethyl orthosilicate ($Si(OC_2H_5)_4$, 98 %, Aldrich), tetrapropylammonium hydroxide ($(CH_3CH_2CH_2)_4N(OH)$, 1.0 M, Sigma-Aldrich), tetrapropylammonium bromide ($(CH_3CH_2CH_2)_4N(Br)$, 98 %, Aldrich), chitosan (molecular weight of 310,000-375,000 Da, Aldrich) and colloidal silica LUDOX® HS-40 (SiO_2, 40 wt%, Sigma-Aldrich) were used as received without further purification. Alumina tubes (50 cm in length) were purchased from Fraunhofer-IKTS (Hermsdorf, Germany).

Pre-treatment of alumina supports

Commercial porous asymmetric α-alumina tubes with an inner layer of γ-phase alumina were used as supports (figure S9a). The pore size of the α- and γ-alumina layers was 200 µm and 60 nm. The outer diameter of the tubes was 10 mm and the wall thickness was 2 mm. The tubes were cut into 2 cm-long or 8 cm-long pieces. The short pieces were used for synthesis probes and characterization studies. The long pieces were employed in single gas permeation experiments. Typically, *support/substrate/tube* will refer to short or both short and long pieces while *membrane* will mean only 8 cm-pieces. Prior to synthesis, the supports were washed with boiling water for 2 h. They were then immersed in acetone under sonication for 15 min. Finally, the substrates were dried at 120 °C overnight. Syntheses were carried out on the inner surface of the supports, and the tubes were wrapped with Teflon tape to avoid product deposition on their external surface.

LUDOX®-treatment of alumina supports

The treatment of the supports with colloidal silica LUDOX® consisted of dipping the bare tubes in the LUDOX® suspension for 45 min. They were then rinsed with deionized water and dried at 200 °C overnight.

Synthesis of silicalite-1 layer

Preparation of silicalite-1 seed suspension

Silicalite-1 seeds were prepared under hydrothermal treatment following the procedure described elsewhere.[54] The seed suspension was prepared by mixing tetrapropylammonium hydroxide (TPAOH), tetraethyl orthosilicate (TEOS) and H_2O in the molar composition 9 TPAOH:25 TEOS:408 H_2O under vigorous stirring at room temperature for 24 h. It was then heated in a Teflon-lined stainless steel autoclave at 100 °C for 24 h. After cooling, silicalite-1 seeds were recovered by centrifugation and washed with deionized water several times until achieving a suspension with pH = 7. The concentration was adjusted to 20 g L^{-1}.

Seeding of supports

Silicalite-1 particles were deposited on the inner cylindrical surface of the supports by a dip-coating procedure. The pH of the seed suspension was adjusted up to 8-9 with TPAOH. The supports were vertically soaked with one end in the filtered suspension for 20 s. After drying at room temperature for 1 h, the tubes were turned 180° and immersed again. This dipping cycle

was repeated three times. After the last immersion, the seeded tubes were thoroughly washed with deionized water to remove the silicalite-1 excess and dried under ambient conditions.

Secondary growth

The synthesis gel was hydrothermally prepared by mixing tetrapropylammonium bromide (TPABr), TEOS, KOH and H_2O in the molar ratio of 1 TPABr:4.5 TEOS:1 KOH:1000 H_2O, as reported by Xomeritakis *et al*.[41] The gel was aged for 24 h under stirring. A support was vertically placed inside a Teflon-lined stainless steel autoclave. The gel was placed in the autoclave and heated at 180 °C in an oven for 24 h. The reaction was carried out under rotation (22 rpm) for long supports. After cooling, the support with the silicalite-1 layer was rinsed with deionized water and dried at room temperature overnight.

Synthesis of bulk silicalite-1 samples

Silicate-1 crystals were prepared under hydrothermal conditions using the molar composition from the seed suspension (8 TPAOH:25 TEOS:408 H_2O). After aging under stirring at room temperature for 24 h, the suspension was transferred to a Teflon-lined stainless steel autoclave which was placed in a preheated oven at 180 °C for 24 h. After cooling, the silicalite-1 crystals were collected by centrifugation, washed three times with deionized water and dried at ambient temperature.

Calcination of silicalite-1 layer and powder

Calcination of the supports after the zeolite layer formation was carried out to remove the TPA^+ template species. Two different temperatures (380 and 450 °C) were tested to study the effect on anchoring MIL-68(Al) crystals. Substrates with the zeolite layer were calcined at the corresponding temperature for 8 h with a step at 100 °C for 1 h for water removal. Heating and cooling ramps of 1 °C min^{-1} were used. The silicalite-1 powder was calcined at 380 or 450 °C in the same conditions as the zeolite layers.

Chitosan coating

As chitosan is a biopolymer insoluble in water but soluble in dilute acidic solutions, it was dissolved in an acetic acid aqueous solution (5 wt%) at a concentration of 1 wt%.[51, 52] Supports were soaked in the chitosan solution for 24 h under static conditions at room temperature. The acetic acid and water were then removed from the chitosan-coated supports by drying at 120 °C overnight with heating and cooling rates of 1 °C min^{-1}.

Synthesis of the MIL-68(Al) layer and powder

The deposition of the MIL-68(Al) was identically performed on bare alumina tubes as well as LUDOX®-, zeolite- and chitosan-coated supports. The MOF layer was prepared following the synthesis conditions reported by Yang *et al*.[28] In a typical synthesis, 0.1098 g of aluminum chloride hexahydrate and 0.1125 g of terephthalic acid (H_2BDC) were mixed in 6.75 mL of *N*,*N*-dimethylformamide (DMF) (0.4392 g, 0.4500 g and 27 mL, respectively, for long tubes). The mixture was stirred for 30 min and a clear solution was obtained. Bare and LUDOX®/silicalite-1/chitosan-coated substrates were vertically placed inside a Teflon-lined autoclave along with

the solution. The autoclave was placed in an oven which was heated at 130 °C for 18.5 h. In the case of long substrates, rotation (22 rpm) was used in order to achieve a uniform layer. After cooling, the support with the MOF or LUDOX®/zeolite/chitosan-MOF layer was washed twice for 60 s with DMF in an ultrasonic bath and dried at room temperature under a funnel to achieve a slow solvent evaporation.

For comparison, bulk MIL-68(Al) was synthesized under the same conditions. After reaction and cooling, the MOF was collected by centrifugation, washed three times with fresh DMF and dried at ambient temperature. As-synthesized MIL-68(Al) is named MIL-68(Al)_as.

Activation of the MIL-68(Al) layers

The supports and membranes with the MIL-68(Al) layer were activated to remove unreacted reagents and trapped solvent molecules from the MOF synthesis. The activation method consisted of two stages: solvent and thermal treatments. In the first, wet supports were soaked in 150 mL of fresh DMF under reflux in a bath at 130 °C for 24 h to dissolve unreacted ligand molecules. Then, the same process was carried out with methanol (MeOH) reducing the temperature down to 60 °C in order to exchange DMF for MeOH. The same volume of solvents was employed for both short (2 cm) and long (8 cm) tubes. The substrates were dried under a funnel at ambient conditions overnight. In the second step, the samples were treated under vacuum for 24 h at 200 °C with heating and cooling rates of 1 °C min^{-1}. In order to determine if the activation process was successful without breaking the long membranes (used in permeation experiments), bulk MIL-68(Al) powders obtained in the corresponding membrane preparation were subjected to the same activation process. The activated MOF products were named MIL-68(Al)_sil and MIL-68(Al)_chi for the MOF/zeolite and MOF/chitosan membranes, respectively.

Figure S9b shows for comparison photographs of the inner surface of supports coated by silicalite-1 seeds, uncalcined and calcined (380 °C) silicalite-1 layer, MIL-68(Al)/silicalite-1, chitosan, MIL-68(Al)/chitosan and activated MIL-68(Al)/chitosan.

Single gas permeation experiments

Single gas permeances were measured *via* the pressure drop method (PDM).[55] Experiments were carried out with N_2, CH_4, CO_2 and H_2 as permeating gases using a transmembrane pressure between 1 and 4 bar at 35 °C. The transmembrane pressure was controlled through a manometer placed in the feed side. The retentate side was closed while the permeate one was open to atmospheric pressure. A stainless steel module was used to contain the membrane. Viton O-rings® at both edges of the membrane sealed the setup to ensure no leaks inside the module. In addition, both ends were sealed with a glazing compound (epoxy adhesive Loctite EA 9492, Henkel) to prevent gas bypass inside the module. Permeance experiments started once the steady state was achieved after about 1 h. Permeance values were calculated from the volumetric flow measured by a soap bubble flow meter. The permeance for a gas *i*, F_i, is described by:

$$F_i = \frac{\dot{n}_i}{A\,\Delta P} \qquad \text{Equation 1}$$

where $\dot{n}_i$ is the molar flow of the permeating gas *i*, *A* is the membrane area and *ΔP* is the transmembrane pressure difference.

Ideal selectivity of gas *i* over gas *j*, $S_{i/j}$, was calculated as the ratio of the single permeances:

$$S_{i/j} = \frac{F_i}{F_j} \qquad \text{Equation 2}$$

Bare alumina tubes, silicalite-1 membranes (before MOF deposition), hybrid MOF/zeolite membranes as well as MIL-68(Al)/chitosan membranes (all the membranes being 8 cm-long) were characterized by means of single gas permeation tests. In some cases, measurements were carried out on two membranes and the permeances obtained were averaged to achieve more accurate values.

The gas transport through porous membranes is governed by a combination of viscous and Knudsen flows.[56] When the pore size of a porous membrane is the same as or smaller than the mean free path of the gas molecules, the gas separation can occur by Knudsen diffusion, where lighter gases permeate faster than heavier gases. Besides, collisions take place principally between gas molecules and pore walls.[56] In viscous or laminar flow, the pore size is larger than the mean free path. In this case, molecule-molecule collisions are dominant.[56, 57] The permeance, *F*, is given by:

$$F = F_K + F'_V P_m \qquad \text{Equation 3}$$

where F_K is the permeance due to Knudsen transport, $F'_V P_m$ is the viscous contribution and P_m is the membrane mean pressure.[56] The viscous and Knudsen contributions were determined as percentages in respect to the total flow at P_m = 1 bar and 35 °C. The viscous flow is related to the existence of large intercrystalline defects, so that a high Knudsen contribution (low viscous percentage) is expected for a high quality membrane.[46] The Knudsen and viscous percentages for the three kinds of membranes prepared in this work are detailed in table S1. The Knudsen selectivity, $\alpha_{Kn,i/j}$ is defined as the square root of the molecular weight of the gas components *j* (Mw_j) and *i* (Mw_i):

$$\alpha_{Kn,i/j} = \sqrt{\frac{Mw_j}{Mw_i}} \qquad \text{Equation 4}$$

Characterization

Scanning electron microscopy (SEM, FEI Inspect F50) was used to examine the materials in powder form. Samples were covered with platinum under vacuum conditions. Environmental scanning electron microscopy (ESEM, Quanta FEG-250 SEM) images were gathered in order to observe the morphology of the deposited crystals as well as to study the cross section of the supports. SEM and ESEM images were taken at a voltage of 5-15 kV. Composition maps of the cross sections were analysed by energy-dispersive X-ray spectroscopy (EDX) using a Quanta FEG-250 SEM microscope. Fourier transform infrared (FTIR, Shimadzu IRAffinity-1) spectra of bulk samples were measured by the KBr disk method in the wavenumber range of 4000-400 cm^{-1} at a resolution of 4 cm^{-1} averaging 20 scans. Attenuated total reflectance Fourier transform infrared spectroscopy (ATR-FTIR, Hyperion 1000) was used to confirm the presence of MIL-68(Al) on the inner tube surface. The ATR-FTIR spectra were collected between 4000 and 600 cm^{-1}

averaging 40 scans with 4 cm^{-1} resolution. Powder X-ray diffraction (PXRD, D-Max Rigaku) patterns of samples were collected at room temperature with a copper anode using a graphite monochromator to select CuKα radiation with λ = 1.5418 Å. Diamond software[58] was employed to create molecular graphics of MIL-68 by means of the MIL-68(Sc) cif file from Mitchell e*t al*.[31] Physisorption isotherms with N_2 at 77 K (Micromeritics TriStar 3000) were measured to determine the BET (Brunauer-Emmett-Teller) surface area of silicalite-1 powder. Prior to the analysis, silicalite-1 was evacuated at 200 °C for 8 h with a heating rate of 10 °C min^{-1}. Test supports (2 cm in length) were broken for characterization.

Acknowledgements

The authors acknowledge financial support from the Spanish Ministry of Economy and Competitiveness (MAT2013-40556-R, MAT2016-77290-R), the Aragón Government (DGA, T05), the European Social Fund (ESF) and FEDER. A. P.-C. also thanks the DGA for a Ph.D. grant. The microscopy work was carried out in the Laboratorio de Microscopías Avanzadas at the Instituto de Nanociencia de Aragón (LMA-INA, Universidad de Zaragoza). The authors would like to acknowledge the use of the Servicio General de Apoyo a la Investigación-SAI (Universidad de Zaragoza).

Keywords

MOF, MIL-68(Al), thin film, linking agent, gas permeation

References

[1] M. Shah, M. C. McCarthy, S. Sachdeva, A. K. Lee, H. K. Jeong, *Ind. Eng. Chem. Res.* **2012**, *51*, 2179-2199.
[2] J. R. Li, J. Sculley, H. C. Zhou, *Chem. Rev.* **2012**, *112*, 869-932.
[3] H. B. T. Jeazet, S. Sorribas, J. M. Roman-Marin, B. Zornoza, C. Téllez, J. Coronas, C. Janiak, *Eur. J. Inorg. Chem*. **2016**, 4363-4367.
[4] K. Sumida, D. L. Rogow, J. A. Mason, T. M. McDonald, E. D. Bloch, Z. R. Herm, T. H. Bae, J. R. Long, *Chem. Rev.* **2012**, *112*, 724-781.
[5] S. Qiu, M. Xue, G. Zhu, *Chem. Soc. Rev.* **2014**, *43*, 6116-6140.
[6] Z. Y. Yeo, S. P. Chai, P. W. Zhu, A. R. Mohamed, *RSC Adv.* **2014**, *4*, 54322-54334.
[7] a) N. Stock, S. Biswas, *Chem. Rev.* **2012**, *112*, 933-969; b) J. Yao, H. Wang, *Chem. Soc. Rev.* **2014**, *43*, 4470-4493; c) A. Perea-Cachero, J. Dechnik, R. Lahoz, C. Janiak, C. Téllez, J. Coronas, *CrystEngComm* **2017**, 19, 1470-1478.
[8] F. Cacho-Bailo, I. Matito-Martos, J. Perez-Carbajo, M. Etxeberria-Benavides, O. Karvan, V. Sebastian, S. Calero, C. Téllez, J. Coronas, *Chem. Sci.* **2017**, *8*, 325-333.
[9] J. Liu, F. Zhang, X. Zou, S. Zhou, L. Li, F. Sun, S. Qiu, *Eur. J. Inorg. Chem.* **2012**, 5784-5790.
[10] H. B. Tanh Jeazet, C. Staudt, C. Janiak, *Dalton Trans.* **2012**, *41*, 14003-14027.
[11] Y. Yoo, Z. P. Lai, H. K. Jeong, *Microporous Mesoporous Mater.* **2009**, *123*, 100-106.
[12] J. Gascon, F. Kapteijn, B. Zornoza, V. Sebastian, C. Casado, J. Coronas, *Chem. Mater.* **2012**, *24*, 2829-2844.
[13] a) C. Serre, F. Millange, C. Thouvenot, M. Nogues, G. Marsolier, D. Louer, G. Ferey, *J. Am. Chem. Soc.* **2002**, *124*, 13519-13526; b) S. Kitagawa, R. Kitaura, S. Noro, *Angew. Chem., Int. Ed.* **2004**, *43*, 2334-2375; c) S. L. Qiu, G. S. Zhu, *Coord. Chem. Rev.* **2009**, *253*, 2891-2911; d) D. Frohlich, S. K. Henninger, C. Janiak, *Dalton Trans.* **2014**, *43*, 15300-15304.
[14] P. Amo-Ochoa, F. Zamora, *Coord. Chem. Rev.* **2014**, *276*, 34-58.
[15] H. J. Park, D. W. Lim, W. S. Yang, T. R. Oh, M. P. Suh, *Chem. – Eur. J.* **2011**, *17*, 7251-7260.

[16] L. M. Huang, H. T. Wang, J. X. Chen, Z. B. Wang, J. Y. Sun, D. Y. Zhao, Y. S. Yan, *Microporous Mesoporous Mater.* **2003**, *58*, 105-114.
[17] D. Y. Hong, Y. K. Hwang, C. Serre, G. Ferey, J. S. Chang, *Adv. Funct. Mater.* **2009**, *19*, 1537-1552.
[18] J. R. Li, R. J. Kuppler, H. C. Zhou, *Chem. Soc. Rev.* **2009**, *38*, 1477-1504.
[19] W. Xuan, C. Zhu, Y. Liu, Y. Cui, *Chem. Soc. Rev.* **2012**, *41*, 1677-1695.
[20] A. Huang, W. Dou, J. Caro, *J. Am. Chem. Soc.* **2010**, *132*, 15562-15564.
[21] A. Huang, H. Bux, F. Steinbach, J. Caro, *Angew. Chem., Int. Ed.* **2010**, *49*, 4958-4961.
[22] Y. Yoo, H. K. Jeong, *Chem. Comm.* **2008**, 2441-2443.
[23] V. V. Guerrero, Y. Yoo, M. C. McCarthy, H. K. Jeong, *J. Mater. Chem.* **2010**, *20*, 3938-3943.
[24] J. G. Nguyen, S. M. Cohen, *J. Am. Chem. Soc.* **2010**, *132*, 4560-4561.
[25] X. Dong, K. Huang, S. Liu, R. Ren, W. Jin, Y. S. Lin, *J. Mater. Chem.* **2012**, *22*, 19222-19227.
[26] K. Barthelet, J. Marrot, G. Ferey, D. Riou, *Chem. Comm.* **2004**, 520-521.
[27] B. Seoane, V. Sebastian, C. Tellez, J. Coronas, *CrystEngComm* **2013**, *15*, 9483-9490.
[28] Q. Yang, S. Vaesen, M. Vishnuvarthan, F. Ragon, C. Serre, A. Vimont, M. Daturi, G. De Weireld, G. Maurin, *J. Mater. Chem.* **2012**, *22*, 10210-10220.
[29] C. Echaide-Gorriz, S. Sorribas, C. Téllez, J. Coronas, *RSC Adv.* **2016**, *6*, 90417-90426.
[30] X. Y. Dong, Q. Liu, A. S. Huang, *J. Appl. Polym. Sci.* **2016**, *133*, 43485.
[31] L. Mitchell, B. González-Santiago, J. P. S. Mowat, M. E. Gunn, P. Williamson, N. Acerbi, M. L. Clarke, P. A. Wright, *Catal. Sci. Technol.* **2013**, *3*, 606-617.
[32] a) E. M. Flanigen, J. M. Bennett, R. W. Grose, J. P. Cohen, R. L. Patton, R. M. Kirchner, J. V. Smith, *Nature* **1978**, *271*, 512-516; b) T. Karbowiak, M. A. Saada, S. Rigolet, A. Ballandras, G. Weber, I. Bezverkhyy, M. Soulard, J. Patarin, J. P. Bellat, *Phys. Chem. Chem. Phys.* **2010**, *12*, 11454-11466.
[33] Z. Y. Yeo, P. W. Zhu, A. R. Mohamed, S. P. Chai, *CrystEngComm* **2014**, *16*, 3072-3075.
[34] Z. P. Lai, M. Tsapatsis, J. R. Nicolich, *Adv. Funct. Mater.* **2004**, *14*, 716-729.
[35] M. Navarro, E. Mateo, B. Diosdado, J. Coronas, *CrystEngComm* **2012**, *14*, 6016-6022.
[36] M. Hunger, *Solid State Nucl. Magn. Reson.* **1996**, *6*, 1-29.
[37] P. R. Palacios, L. De Los Santos Valladares, A. Bustamante, J. C. Gonzalez, *Rev. Soc. Quim. Peru* **2012**, *78*, 198-207.
[38] G. H. Kühl in *Catalysis and zeolites: fundamentals and applications* (Eds.: J. Weitkamp, L. Puppe), 1st ed., Springer-Verlag Berlin Heidelberg, Berlin, **1999**, pp. 81-197.
[39] L. Tosheva, B. Mihailova, V. Valtchev, J. Sterte, *Microporous Mesoporous Mater.* **2000**, *39*, 91-101.
[40] C. Volkringer, M. Meddouri, T. Loiseau, N. Guillou, J. Marrot, G. Ferey, M. Haouas, F. Taulelle, N. Audebrand, M. Latroche, *Inorg. Chem.* **2008**, *47*.
[41] G. Xomeritakis, S. Nair, M. Tsapatsis, *Microporous Mesoporous Mater.* **2000**, *38*, 61-73.
[42] O. de la Iglesia, S. Irusta, R. Mallada, M. Menendez, J. Coronas, J. Santamaria, *Microporous Mesoporous Mater.* **2006**, *93*, 318-324.
[43] a) Y. Yoo, H. K. Jeong, *Cryst. Growth Des.* **2010**, *10*, 1283-1288; b) K. A. McDonald, J. I. Feldblyum, K. Koh, A. G. Wong-Foy, A. J. Matzger, *Chem. Comm.* **2015**, *51*, 11994-11996.
[44] Z. Y. Yeo, S. P. Chai, P. W. Zhu, A. R. Mohamed, *Microporous Mesoporous Mater.* **2014**, *196*, 79-88.
[45] S. Sorribas, B. Zornoza, C. Téllez, J. Coronas, *J. Membr. Sci.* **2014**, *452*, 184-192.
[46] O. de la Iglesia, M. Pedernera, R. Mallada, Z. Lin, J. Rocha, J. Coronas, J. Santamaria, *J. Membr. Sci.* **2006**, *280*, 867-875.
[47] M. P. Pina, R. Mallada, M. Arruebo, M. Urbiztondo, N. Navascues, O. de la Iglesia, J. Santamaria, *Microporous Mesoporous Mater.* **2011**, *144*, 19-27.
[48] T. C. Bowen, R. D. Noble, J. L. Falconer, *J. Membr. Sci.* **2004**, *245*, 1-33.
[49] C. A. Murray, J. R. Dutcher, *Biomacromolecules* **2006**, *7*, 3460-3465.
[50] M. Dash, F. Chiellini, R. M. Ottenbrite, E. Chiellini, *Prog. Polym. Sci.* **2011**, *36*, 981-1014.

[51] M. Zhou, X. Liu, B. Zhang, H. Zhu, *Langmuir* **2008**, *24*, 11942-11946.
[52] S. Zhou, X. Zou, F. Sun, F. Zhang, S. Fan, H. Zhao, T. Schiestel, G. Zhu, *J. Mater. Chem.* **2012**, *22*, 10322-10328.
[53] Y. X. Hu, X. L. Dong, J. P. Nan, W. Q. Jin, X. M. Ren, N. P. Xu, Y. M. Lee, *Chem. Comm.* **2011**, *47*, 737-739.
[54] M. P. Bernal, PhD thesis, University of Zaragoza, **2001**.
[55] C. Algieri, P. Bernardo, G. Barbieri, E. Drioli, *Microporous Mesoporous Mater.* **2009**, *119*, 129-136.
[56] K. Keizer, R. J. R. Uhlhorn, R. J. Vanvuren, A. J. Burggraaf, *J. Membr. Sci.* **1988**, *39*, 285-300.
[57] a) H. Shehu, E. Okon, E. Gobina, *World Congr. Eng. 2015 Vol. II,* **2015**, 1225-1229; b) H. Kita, in *Materials Science of Membranes for Gas and Vapor Separations* (Eds.: Y. Yampolskii, I. Pinnau, B. Freeman), John Wiley & Sons Ltd, West Sussex, **2006**, pp. 337-354.
[58] H. Putz and K. Brandenburg, Diamond - Crystal and Molecular Structure Visualization**,** Brandenburg GbR, Bonn, Germany, 2016.